



OPEN

SUBJECT AREAS:

ELECTRICAL AND
ELECTRONIC
ENGINEERING

APPLIED PHYSICS

THERMOELECTRICS

Breaking the trade-off between thermal and electrical conductivities in the thermoelectric material of an artificially tilted multilayer

Akihiro Sakai¹, Tsutomu Kanno¹, Kouhei Takahashi¹, Hiromasa Tamaki¹, Hideo Kusada¹, Yuka Yamada¹ & Hiroya Abe²Received
3 June 2014Accepted
30 July 2014Published
15 August 2014Correspondence and
requests for materials
should be addressed to
A.S. (sakai.aki-hiro@
jp.panasonic.com)¹Advanced Technology Research Laboratories, Panasonic Corporation, Kyoto 619-0237, Japan, ²Joining and Welding Research Institute, Osaka University, Osaka 567-0047, Japan.

Breaking the trade-off between thermoelectric (TE) parameters has long been demanded in order to highly enhance its performance. Here, we report the ‘trade-off-free’ interdependence between thermal conductivity (κ) and resistivity (ρ) in a TE/metal tilted multilayer and significant enhancement of TE power generation based on the off-diagonal thermoelectric (ODTE) effect, which generates transverse electrical current in response to vertical thermal current. ρ and κ can be simultaneously decreased by setting charge flow along more-electrically conductive layer and thermal flow across less-thermally conductive perpendicular direction by decreasing the tilting angle. Moreover, introducing porosity in the metal layer enables to decrease in κ without changing ρ , because the macroscopic ρ and κ of the tilted multilayer is respectively governed by the properties of the TE material and the metal with large dissimilarity. The obtained results reveal new strategies for developing trade-off-free TE materials, which will stimulate practical use of TE conversion for waste-heat recovery.

To reduce worldwide primary energy consumption, much attention is now focused on power generation from enormous amounts of low-temperature waste heat. Its main media is hot water and low pressure steam at temperatures below 200°C commonly found in plants, automobiles, geothermal areas and other locations. Thermoelectric (TE) technology is a suitable solution for waste heat recovery since it can directly convert such low-grade thermal energy to electricity and also construct a power generator into a compact system.

The performance of TE materials is quantified by the figure of merit $ZT = S^2 T \rho^{-1} \kappa^{-1}$ where the individual TE parameters depends on the carrier density as shown schematically in Fig. 1a (Seebeck coefficient: S , electric resistivity: ρ , thermal conductivity: κ and absolute temperature: T)¹. Increase in carrier density gives advantages to decreasing ρ and disadvantage to increasing κ and decreasing of S (not shown). During the past half century, the ‘trade-off’ between the TE parameters has hampered serious improvement of ZT . It has long been demanded to find a way to optimize the TE parameters independently. A recent common approach to overcome the trade-off is to form a so-called ‘PGEC’ (Phonon glass Electron crystal) by nanoscale structuring^{2–6}. The interrelation between ρ and κ appears to be almost independent and enhances $\rho^{-1} \kappa^{-1}$ in ZT as schematically shown in Fig. 1b. By tuning the density of the scattering centres, we can selectively scatter phonons with longer mean free paths, and hence, can decrease κ without largely degrading ρ ^{4,5}. However, this PGEC approach can generally only decrease κ , and the effective range of selective scattering is limited by differences in the phonon and charge mean free path of the material. As an alternative approach beyond the PGECs, here we propose a way to decouple the thermal and charge conducting paths by using the off-diagonal TE (ODTE) effect. This effect typically appears in multilayers with alternate stacks of dissimilar materials such as a TE material and a pure metal^{7–15}. In these multilayer materials, we can change the TE parameters individually and enhance the performance of TE generation. The macroscopic TE properties of these TE/metal multilayers are highly anisotropic between layer parallel and perpendicular directions: $\kappa_{\perp} \ll \kappa_{\parallel}$, $\rho_{\perp} \gg \rho_{\parallel}$ and $S_{\perp} \gg S_{\parallel}$. The thermal and electrical anisotropies originate from the different ways of stack dissimilar components in series and in parallel toward the directions of thermal and charge current. In the layer parallel direction, we observe high thermal and electrical conductivity nearly as high as those of the pure metal components. In contrast, we observe low conductivity similar to the TE material in

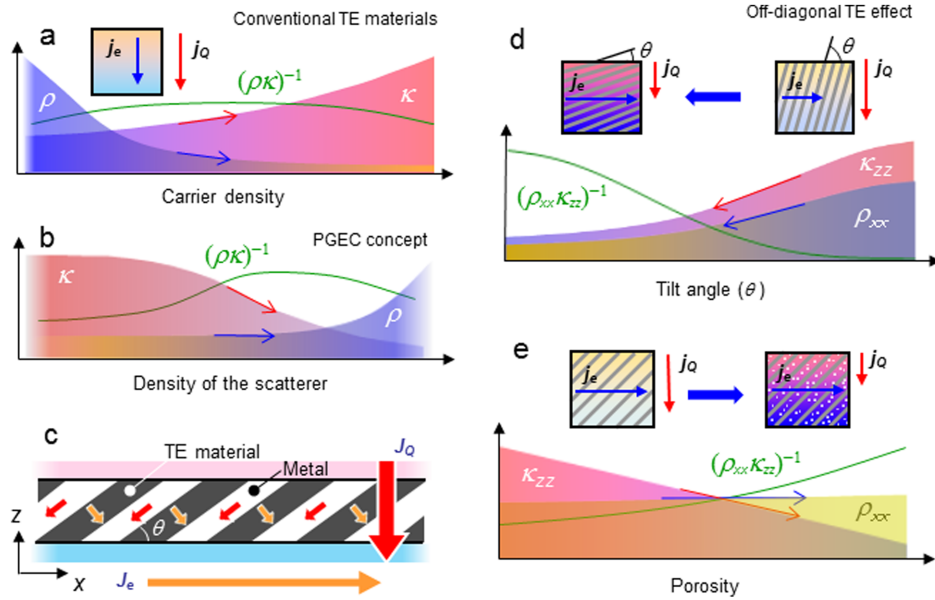


Figure 1 | Concept of trade-off-free interrelation between κ and ρ using the ODTE effect. The behaviours of thermal conductivity (κ), resistivity (ρ) and $\rho^{-1}\kappa^{-1}$ of a thermoelectric (TE) material controlled by (a) carrier-density and (b) PGEC concept. (c) Schematic illustration of the off-diagonal TE effect in a tilted artificial multilayer of a TE material and metal. The large arrows show the macroscopic thermal (red) and charge (orange) currents. Also shown are two mechanisms for improving $\rho^{-1}\kappa^{-1}$ in the multilayer: (d) simultaneous decrease in κ and ρ by changing the tilt angle and (e) independent decrease in κ and constant ρ by increasing the porosity of the metal.

the layer perpendicular direction. The TE properties of the multilayer in the layer parallel ($S_{//}$, $\kappa_{//}$ and $\rho_{//}$) and perpendicular (S_{\perp} , κ_{\perp} and ρ_{\perp}) are expressed in

$$\rho_{//} = \frac{1}{\frac{a}{\rho_M} + \frac{1-a}{\rho_{TE}}} \quad \kappa_{//} = a\kappa_M + (1-a)\kappa_{TE} \quad S_{//} = \frac{\frac{(1-a)S_{TE}}{\rho_{TE}} + \frac{aS_M}{\rho_M}}{\frac{1-a}{\rho_{TE}} + \frac{a}{\rho_M}} \quad (1)$$

$$\rho_{\perp} = a\rho_M + (1-a)\rho_{TE} \quad \kappa_{\perp} = \frac{1}{\frac{a}{\kappa_M} + \frac{1-a}{\kappa_{TE}}} \quad S_{\perp} = \frac{\frac{(1-a)S_{TE}}{\kappa_{TE}} + \frac{aS_M}{\kappa_M}}{\frac{1-a}{\kappa_{TE}} + \frac{a}{\kappa_M}} \quad (2)$$

Eqs. (1) and (2)^{7,8,10,11}, where S_{TE} , κ_{TE} and ρ_{TE} are the TE properties of TE material and S_M , κ_M and ρ_M are the TE properties of the metal and a is the volume occupancy by the metal layer. The ODTE effect is developed in such an anisotropic material by tilting the laminated planes by θ against the material surface normal. This then generates a transverse TE current (J_e) in response to a vertical thermal current (J_Q) as shown in Fig. 1c. Finite element method analysis revealed that a microscopic J_Q flow diagonally in each layer, and thus, generating diagonal J_e in each layers as well, which leads to generation of a macroscopically transverse J_e as a whole^{10,15}. TE parameters in tilted multilayer are theoretically formulated by a tensor as Eq. (3)¹³, where A corresponds to each one of the TE parameters (S , ρ and κ) and θ is the tilting angle. In the ODTE effect, the figure of merit is described as $Z_{xz}T = S_{xz}^2 T \kappa_{zz}^{-1} \rho_{xx}^{-1}$ using ρ_{xx} , κ_{zz} and S_{xz} ^{10-12,14}. The TE properties in the multilayer can be optimized by controlling θ and combination of dissimilar components, which is a different optimizing way from the conventional TE materials. In this paper, we theoretically

$$\begin{pmatrix} A_{xx} & A_{xz} \\ A_{zx} & A_{zz} \end{pmatrix} = \begin{pmatrix} A_{\parallel} \cos^2 \theta + A_{\perp} \sin^2 \theta & \frac{1}{2}(A_{\parallel} - A_{\perp}) \sin 2\theta \\ \frac{1}{2}(A_{\parallel} - A_{\perp}) \sin 2\theta & A_{\parallel} \sin^2 \theta + A_{\perp} \cos^2 \theta \end{pmatrix} \quad (3)$$

and experimentally demonstrate trade-off-free interdependences of TE parameters in a $\text{Bi}_{0.5}\text{Sb}_{1.5}\text{Te}_3/\text{Ni}$ artificially tilted multilayer and significant enhancements in $Z_{xz}T$ and output power, accomplished by controlling θ and degree of material porosity.

Equation (3) shows there are two mechanisms which possibly yield trade-off-free interdependences between ρ_{xx} and κ_{zz} : (1) the coefficient of $A_{//}$ and A_{\perp} is opposite for ρ_{xx} and κ_{zz} . We can simultaneously decrease ρ_{xx} to $\rho_{//}$ and κ_{zz} to κ_{\perp} by decreasing θ ($\sin^2 \theta \ll \cos^2 \theta$); and (2) the extremely large difference between $A_{//}$ and A_{\perp} in ρ_{xx} and κ_{zz} . κ_{zz} is governed by $\kappa_{//}$, which can be approximated by the thermal property of the metal. In contrast, ρ_{xx} is governed by ρ_{\perp} , which can be approximated by the electrical properties of TE material. In Fig. 1d and 1e, we schematically show how to introduce the trade-off-free interdependences according to mechanisms (1) and (2), respectively. In Fig. 1d, by decreasing θ , we see that the laminated planes become more parallel to the direction of the transverse J_e , and thereby, ρ_{xx} approaches to $\rho_{//}$. Simultaneously, the direction of J_Q becomes closer to orthogonal to the laminated planes, which decreases κ_{zz} to κ_{\perp} . In such a way, we can realize a material with κ , similar to TE materials, and higher electrical conductivity, similar to pure metals. Figure 1e shows that increasing the porosity and changing κ of the metal layer yields reduction in κ_{zz} without changing ρ_{xx} of the multilayer. This independent change occurs because ρ_{xx} of the multilayer is mainly governed by ρ of the TE material and κ_{zz} is mainly governed by κ in the metal. The interrelation from mechanisms (1) and (2) simultaneously decrease κ_{zz} and ρ_{xx} as well as decrease κ_{zz} without degrading ρ_{xx} respectively, which can largely increase $\kappa_{zz}^{-1}\rho_{xx}^{-1}$ in $Z_{xz}T$.

Results and Discussion

We have fabricated tilted multilayers of $\text{Bi}_{0.5}\text{Sb}_{1.5}\text{Te}_3$ (BST) and Nickel (Ni) in a tubular structure using spark plasma sintering (SPS) and then measured the thermal and electric properties¹⁶. A tilted layer structure is observed in the cross-section of the tubular shaped measured sample with a thickness ratio $t_{\text{BST}}/t_{\text{Ni}} \sim 1$ as depicted in Fig. 2. The optical micrograph in the inset of Fig. 2 reveals an existence of joining layer which assures a fine mechanical and electrical junction between the layers. A typical size of the tubular sample is 11 cm-long with an outer and an inner diameter of 14 and 10 mm, respectively. We performed thermal and electrical measurements in custom equipment that mimicked a shell/tube heat exchanger introducing a temperature difference (ΔT) between tube inside

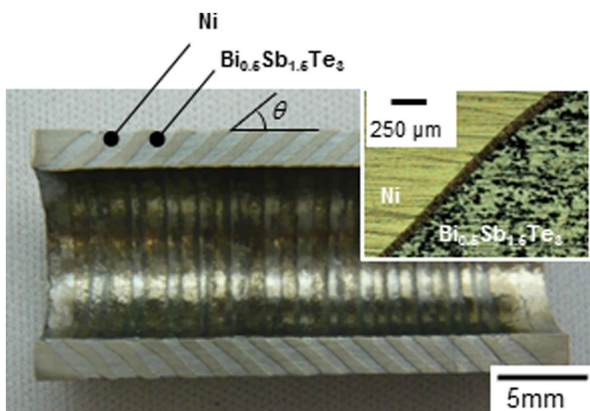


Figure 2 | Cross-section photograph of a tubular tilted multilayer. The tilted multilayer of $\text{Bi}_{0.5}\text{Sb}_{1.5}\text{Te}_3$ and Ni is fabricated by the SPS method. The inset shows optical image around the junction between the two layers.

and outside. The ΔT was maintained by flowing hot water (95°C and 20 L min^{-1}) in the inner side of the BST/Ni tube, and chilled water (10°C and 20 L min^{-1}) in the outer side of the BST/Ni tube.

Dependence on layer tilt angle. The simultaneous decrease in ρ_{xx} and κ_{zz} is theoretically demonstrated by their θ dependences in the multilayer. We can favourably decrease ρ_{xx} and κ_{zz} to ρ_{\parallel} and κ_{\perp} with lowering θ as already shown in the Fig. 1d. To quantitatively elucidate such an interrelation and its effect on $Z_{xz}T$, we calculated the θ dependence of TE parameters and $Z_{xz}T$ based on Eq. (3). The theoretical result reveals more than 90% decrease in both κ_{zz} ($25.4 \rightarrow 2.1 \text{ Wm}^{-1}\text{K}^{-1}$) and ρ_{xx} ($0.73 \rightarrow 0.04 \text{ m}\Omega\text{cm}$) with lowering θ from 90° to 0° in Fig. 3a. This simultaneous decrease in κ and ρ is in contrast with the interrelations in the ordinal TE materials shown in Fig. 1a and 1b. Consequently, $Z_{xz}T$ enhances with decreasing θ ;

$Z_{xz}T$ of 0.4 at $\theta \sim 10^\circ$, as shown in Fig. 3b. In this calculation, we used the TE parameters (S , ρ and κ) of pelletized BST and Ni fabricated by the same SPS condition as before: 500°C and 50 MPa . ($\text{Bi}_{0.5}\text{Sb}_{1.5}\text{Te}_3$; $S \sim 210 \mu\text{V/K}$, $\rho \sim 1.2 \text{ m}\Omega\text{cm}$ and $\kappa \sim 1.1 \text{ Wm}^{-1}\text{K}^{-1}$; Ni; $S \sim -20 \mu\text{V/K}$, $\rho \sim 17 \mu\Omega\text{cm}$ and $\kappa \sim 51 \text{ Wm}^{-1}\text{K}^{-1}$ at room temperature).

We experimentally demonstrate the reduction in both ρ_{xx} and κ_{zz} and enhancement of output power in the θ dependence. We found that the resistance monotonically decreased from 6.7 to 2.4 $\text{m}\Omega$ as θ decreased from 55° to 23° , as shown in Fig. 3c. These results are consistent with the behavior of ρ_{xx} shown in Fig. 3a. We also show in Fig. 3c the θ dependence of the exchanged thermal power (Q). The values of Q were experimentally obtained by the relation of $Q = C_w \rho_w F_{cw} T_{\text{diff}}$, where C_w and ρ_w is the heat capacity and density of the water, F_{cw} is the cold water flowing rate and T_{diff} is the ΔT between cold water inlet and outlet. Here we see that Q monotonically decreases from 1.8 to 1.0 kW with decreasing θ as shown in Fig. 3c. This behavior implies that κ_{zz} actually decreases with decreasing θ . We note that Q is expressed by the relation of $Q = UA\Delta T$, where U and A is the overall thermal transfer coefficient and heat transfer surface area, respectively^{15,17}. In this condition, the thermal resistance (R) along the tube radial direction is described as $(UA)^{-1} = R_H + R_{\text{tube}} + R_c$ where R_H and R_c is the hot and the cold side interfacial thermal resistance, respectively, and R_{tube} is the bulk thermal resistance of the BST/Ni tube. Assuming that R_H and R_c are similar between the fabricated samples, the change in the overall thermal transfer coefficient should largely owe to of the change in R_{tube} , namely the values of κ_{zz}^{-1} . The monotonic decrease in the electrical resistance and Q thus demonstrate the reduction in both ρ_{xx} and κ_{zz} and breaking the trade-off interrelation. The decrease in κ_{zz} by decreasing θ is also demonstrated by the increase in voltage as shown in Fig. 3d. In the θ dependence of generated voltage, we observe values ranging from 0.2–0.28 V with a peak at $\theta \sim 30^\circ$, which is shifted away from the $-S_{xz}$ maximum around 45° as shown

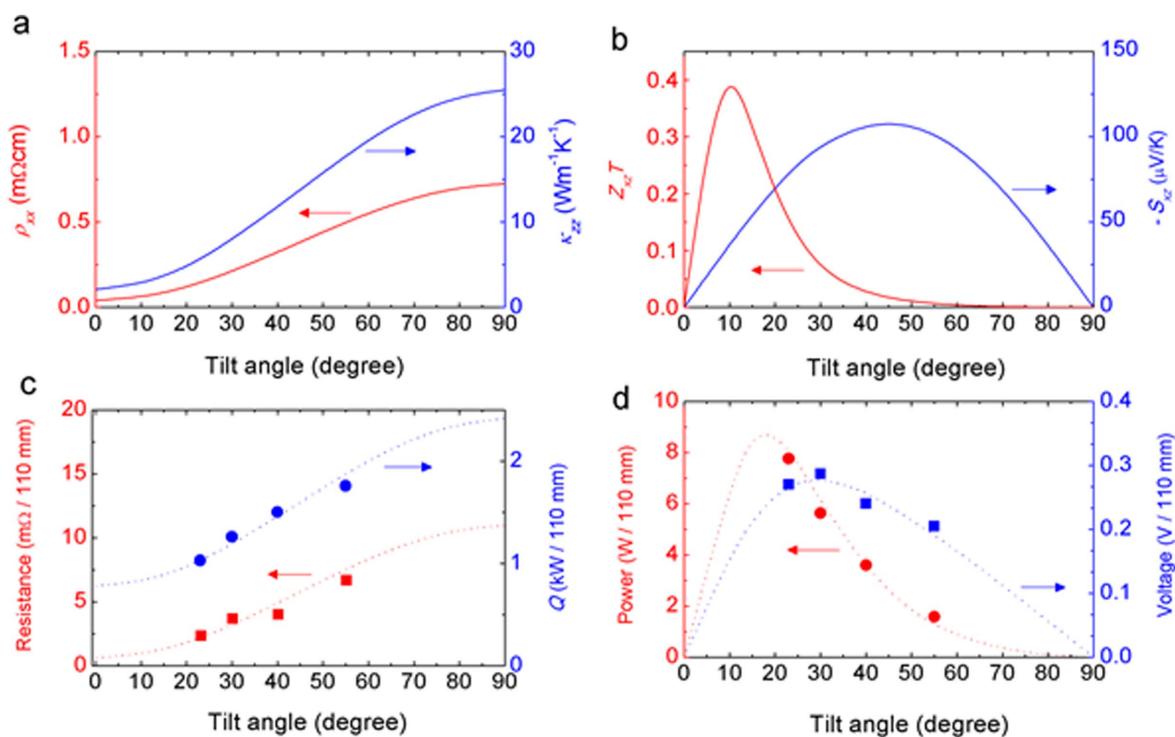


Figure 3 | Theoretically and experimentally demonstrated simultaneous decrease in κ_{zz} and ρ_{xx} and enhancement of TE performance by varying the tilt angle. (a) Theoretical tilt-angle dependence of κ_{zz} and ρ_{xx} and (b) $-S_{xz}$ and $Z_{xz}T$ derived from Eq. (3). (c) Experimentally obtained resistance and exchanged thermal power as a function of tilt angle. (d) Experimentally obtained generated voltage and output power in a 11 cm-long tubular BST/Ni tilted multilayer as a function of tilt angle. The dashed lines in (c) and (d) show the fitting curves based on theoretical calculation.



in Fig. 3b. This again is a signature of decrease in κ_{zz} by decreasing θ . The simultaneous decrease in ρ and κ then steeply and significantly enhanced the output power up to 7.8 W at $\theta \sim 23^\circ$ as shown in Fig. 3d.

Porosity dependence. The independent interrelation between κ_{zz} and ρ_{xx} is theoretically examined by varying the TE properties of each layer component, as already shown in Fig. 1e. κ_{zz} and ρ_{xx} of the multilayer are respectively governed by the properties of Ni and BST, which allowed us to independently control the two quantities. We have investigated how porosity in either layer of BST and Ni affects the multilayer's TE behaviour based on Eq. (3). In this calculation, we assumed that the TE parameters in the Eqs. (1) and (2) varies with porosity and obey the following relations: $\kappa \sim (1-p) \kappa_0$ and $\rho \sim \rho_0 / (1-p)$. Here p is the degree of porosity expressed as $p = (d_0 - d)/d_0$ where d is the density of the respective porous Ni or BST layer and d_0 , κ_0 , ρ_0 , and S_0 are the properties of the fully densified components. ($\text{Bi}_{0.5}\text{Sb}_{1.5}\text{Te}_3$; $d_0 \sim 6.8 \text{ g/cm}^3$, $\rho_0 \sim 1.2 \text{ m}\Omega\text{cm}$, $\kappa_0 \sim 1.1 \text{ Wm}^{-1}\text{K}^{-1}$ and $S_0 \sim 210 \text{ }\mu\text{V/K}$, Ni; $d_0 \sim 8.9 \text{ g/cm}^3$, $\rho_0 \sim 7 \text{ }\mu\Omega\text{cm}$, $\kappa_0 \sim 90 \text{ Wm}^{-1}\text{K}^{-1}$ and $S_0 \sim -20 \text{ }\mu\text{V/K}$ at room temperature). The calculated results show almost independent behaviours between κ_{zz} and ρ_{xx} on p by introducing porosity in either the Ni layer or the BST layer as shown in Fig. 4a. Increasing p of the Ni layer (red solid lines) decreases κ_{zz} and barely changes ρ_{xx} . In contrast, increasing p of the BST layer (blue solid lines) barely changes κ_{zz} and increases ρ_{xx} . These results predict that κ_{zz} and ρ_{xx} in the multilayer are indeed governed by the Ni and BST properties, respectively. We found that the TE parameter variations by introducing porosity in the Ni layer can increase $Z_{xx}T$. Figure 4b shows that $Z_{xx}T$ increases with increasing p over the whole investigated range because ρ_{xx} remains unchanged and κ_{zz} favourably decreases with increasing p in the Ni layer. In contrast, we found that $Z_{xx}T$ monotonically decreases with increasing p in the

BST layer because κ_{zz} remains unchanged and ρ_{xx} unfavourably increases. We therefore see that introducing porosity does not always enhance $Z_{xx}T$. In the case of BST/Ni multilayers, manufacturing porous structure only in the Ni layer is necessary for higher power generation.

By introducing Ni porosity, we experimentally show the independent interrelation between κ and ρ , and enhanced power generation in the BST/Ni multilayer. Figure 4c summarizes the p dependence of electrical resistance, voltage, and the output power of the porous BST/Ni multilayer tube. We see that the measured resistance was almost constant at $\sim 3.5 \text{ m}\Omega$ over the range of p . On the other hand, the voltage independently increased from 260 to 305 mV with increasing p of the Ni layer. It is reasonable to consider that increase in p of the Ni layer decreased κ_{zz} of the entire multilayer while barely impacting ρ_{xx} , which is consistent with the prediction in Fig. 4a. As a result, the output power increased to 6.6 W in the 11-cm-long tube. Provided that p could be further increased, it appears the output power could be further enhanced according to the theoretical result in Fig. 4b. In this measurement, we used the multilayer with a porous Ni layer controlled by the pressure (P_{SPS}) in the SPS sintering. Figure 4d and 4e show transmission electron microscopy (TEM) images of the dense BST and porous Ni layers, respectively, in the multilayer fabricated by SPS at 500°C and 50 MPa. These micrographs revealed porosity only in the Ni layer. This contrastive texture has been caused by differences in the optimal sintering temperature of BST and Ni. The volume fraction of porosity in the Ni increased from 8 to 50% with decreasing P_{SPS} and we simultaneously observe the decreasing κ and increasing ρ in doubly. Table 1 lists the details of P_{SPS} dependence of densification (d and p) and consequent variations in κ and ρ in the Ni.

Enhancement of the power generation. We summarize the enhancement of output power (P) and efficiency (η) of the fabricated

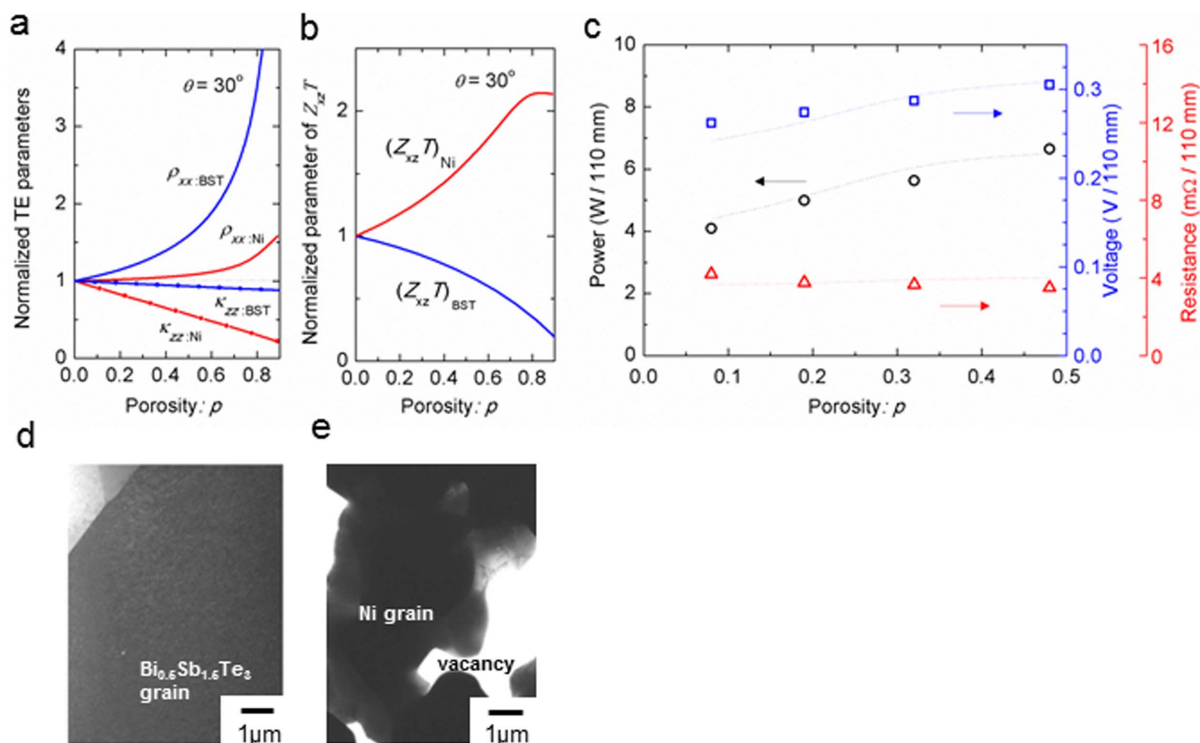


Figure 4 | Theoretically and experimentally demonstrated independent control of κ_{zz} and ρ_{xx} , and its enhancement of performance by introducing Ni porosity. (a) Theoretical porosity effects on (a) κ_{zz} , ρ_{xx} and (b) $Z_{xx}T$ of the $\text{Bi}_{0.5}\text{Sb}_{1.5}\text{Te}_3$ (red) and Ni (blue) layers. (c) Experimentally obtained resistance, generated voltage and output power of a 11-cm long tubular BST/Ni tilted multilayers. The dashed lines show the fitting curves based on theoretical calculation. Also shown are the TEM images of (b) the $\text{Bi}_{0.5}\text{Sb}_{1.5}\text{Te}_3$ layer and (c) the Ni layer of the BST/Ni multilayer fabricated by SPS at 500°C and 50 MPa under vacuum.



Table 1 | P_{SPS} dependence of the Ni density, degree of the porosity, and ρ and κ at room temperature of pelletized Ni samples fabricated at the same SPS condition used for fabricating the BST/Ni tube

Ni (SPS pressure)	Density (g/cm ³)	ρ	ρ ($\mu\Omega$ cm)	κ (W/mK)
30 MPa	6.0	0.48	21	40
50 MPa	6.7	0.32	17	51
100 MPa	7.5	0.19	11.3	67
150 MPa	8.2	0.08	9.7	80

multilayers. We experimentally suppressed κ_{zz} largely by 73% without degrading ρ_{xx} in the multilayer through the optimizations by the trade-off-free interdependences. In an 11-cm long BST/Ni multilayer tube, P significantly increased to a maximum of 7.9 W as shown in Fig. 5a. The power density per heat transfer area reached as high as 2.5 kW/m² with a relatively small $\Delta T = 85$ K at temperatures below 100°C. In Fig. 5b, η ($\eta = P/Q$) of the multilayer also steeply increased up to 0.83% due to increase in P and decrease in Q as shown in Fig. 5c. The reduction in Q originated from the decrease in κ_{zz} of the multilayer. The remarkable feature in our results is the high capability of the multilayer to capture heat effectively ($Q \sim 0.9$ –1.8 kW) and to generate high electric power. The highly heat conductive Ni layer (40 ~ 80 Wm⁻¹K⁻¹) yields an excellent heat exchange property with a maximum Q of 1.8 kW. These high Q values go far beyond the conventional TE devices and make it possible to generate large P in spite of the relatively low η , that is, low $Z_{xx}T$ as shown in the Fig. 3b. From a practical perspective, we can use this material as a bifunctional TE device with efficient heat exchange and high power generation in a standard heat exchanger¹⁸. Note that, to achieve high P , it is important to control κ_{zz} of the multilayer. According to Fig. 5a, $\kappa_{zz} \sim 5$ Wm⁻¹K⁻¹ is desirable in the BST/Ni multilayer. We found the differences in peak position between the variances of P and η because Q is also κ_{zz} -dependent. This result shows that to achieve higher power generation, it is more important to control κ_{zz} appropriately rather than to enhance $Z_{xx}T$ simply by decreasing κ_{zz} of the multilayer.

In this work, we proposed two following approaches to achieve a trade-off-free interrelation between κ and ρ using the ODTE effect in a TE/metal tilted multilayer. (1) Decreasing both κ and ρ by directing J_Q and J_e simultaneously towards the favourable thermally less conductive and electrically more conductive direction. (2) Independently varying κ_{zz} and ρ_{xx} given that κ_{zz} and ρ_{xx} are governed by the properties of Ni and BST, respectively. Theoretical and experimental results validated these proposed approaches and suggested the potential of BST/Ni artificially tilted multilayers for high power generation. Through these optimizations, we demonstrated that κ_{zz} and ρ_{xx} can be suppressed largely, and significantly increase the output power and efficiency to 2.5 kW/m² and 0.83%, respectively, with a relatively small $\Delta T \sim 85$ K at temperature below 100°C. Present findings resolve the conflict between κ and ρ and establish sure design strategies applicable to all effective TE/metal tilted multilayers. The excellent heat exchange capability and high power generation in this multilayer provides an innovative TE application for power generator in the heat exchange system using enormous low temperature waste heat.

Methods

Fabrication of the tubular tilted multilayers. We have fabricated the tubular shaped tilted multilayer using BST and Ni by spark plasma sintering (SPS) method. This method allows sintering powders, joining two materials and tubular shaping simultaneously. To obtain the tilted multilayer structure, we alternately stacked compacted powders of BST and Ni with tilting along the axial direction before sintering. We used cold pressing to compact the powders into a conical ring, which allowed us to easily stack the layers and achieve a uniform tilt angle. The tilt angle was controlled by the tapered angle of the conical rings (15° ~ 45°). SPS sintering was performed at a fixed temperature ~ 500°C and pressures ~ 30–150 MPa under

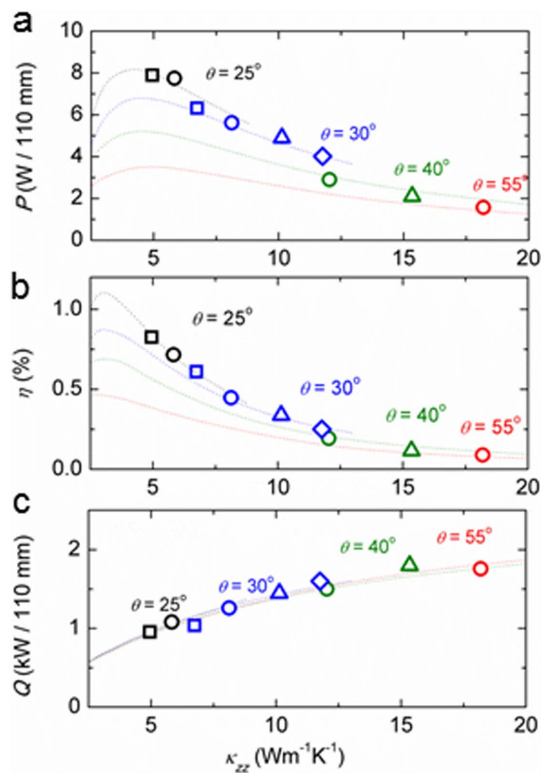


Figure 5 | Summary of performance enhancement in the fabricated multilayer by trade-off free optimizations. Experimentally obtained (a) output power (P), (b) efficiency (η) and (c) thermal exchange power (Q) of the fabricated multilayers as a function of κ_{zz} .

vacuum. The fabricated tubular composites were typically 35 mm long. The cross-section of the sample shows a well-defined tilted layered structure. The composite exhibited no cracks or coarsened voids and had high mechanical stability. We produced 110-mm-long TE tubes by joining four of these tubular composites with Sn-Bi solder paste.

Experimental setup to measure the TE properties of the tilted multilayers. The thermal (exchange thermal power) and electric (resistivity and voltage) measurements were performed using a custom equipment, which simulated a standard shell/tube heat exchanger. The temperature difference between inside and outside of the tube was maintained by flowing hot and cold water, which was controlled by a liquid heater and a chiller unit. The actual water temperatures were measured by a thermocouple sensor attached to the apparatus. Water flow meters were placed in the cold and hot water lines. Resistance and voltage were measured using Cu electrodes, screwed into the exchanger unit to make the electric contact between the materials of BST/Ni.

- Snyder, G. J. & Toberer, E. S. Complex thermoelectric materials. *Nature Mater.* **7**, 105–114 (2008).
- Slack, G. A. [New Materials and Performance Limits for Thermoelectric Cooling]. *Handbook of Thermoelectrics* [Rowe, D.M. (ed.)] [407–440] (CRC press, UK, 1994).
- Sales, B. C. *et al.* Filled skutterudite antimonides: Electron crystals and phonon glasses. *Phys. Rev. B* **56**, 15081–15089 (1997).
- Hochbaum, A. I. *et al.* Enhanced thermoelectric performance of rough silicon nanowires. *Nature* **451**, 163–167 (2008).
- Boukai, A. I. *et al.* Silicon nanowires as efficient thermoelectric materials. *Nature* **451**, 168–171 (2008).
- Poudel, B. *et al.* High-thermoelectric performance of nanostructured bismuth antimony telluride bulk alloys. *Science* **320**, 634–638 (2008).
- Kyarad, A. & Lengfellner, H. Al-Si multilayers: A synthetic material with large thermoelectric anisotropy. *Appl. Phys. Lett.* **85**, 5613–5615 (2004).
- Fischer, K., Stoiber, C., Kyarad, A. & Lengfellner, H. Anisotropic thermopower in tilted metallic multilayer structures. *Appl. Phys. A* **78**, 323–326 (2004).
- Kyarad, A. & Lengfellner, H. Transverse Peltier effect in tilted Pb-Bi₂Te₃ multilayer structures. *Appl. Phys. Lett.* **89**, 192103 (2006).
- Kanno, T. *et al.* Enhancement of transverse thermoelectric power factor in tilted Bi/Cu multilayer. *Appl. Phys. Lett.* **94**, 061917 (2009).



11. Goldsmid, H. J. Synthetic transverse thermoelements made from porous bismuth telluride and single crystal bismuth. *phys. stat. sol. (a)* **205**, 2966–2969 (2008).
12. Reitmaier, C., Walther, F. & Lengfellner, H. Power generation by the transverse Seebeck effect in Pb-Bi₂Te₃ multilayers. *Appl. Phys. A* **105**, 347–349 (2011).
13. Snarskii, A. A. & Bulat, L. P. [Anisotropic Thermoelements]. *Thermoelectrics Handbook: Macro to Nano*. [Rowe, D.M. (ed)] [45-1–45-11] (CRC press, Boca Raton, 2006).
14. Goldsmid, H. J. Application of the Transverse Thermoelectric Effects. *J. Electron. Mater.* **40**, 1254 (2011).
15. Kanno, T. *et al.* Tailoring effective thermoelectric tensors and high-density power generation in a tubular Bi_{0.5}Sb_{1.5}Te₃/Ni composite with cylindrical anisotropy. *Appl. Phys. Lett.* **101**, 011906 (2012).
16. Sakai, A. *et al.* Enhancement in Performance of the Tubular Thermoelectric Generator (TTEG). *J. Electron. Mater.* **42**, 1612 (2013).
17. Boehm, R. F. [Heat and Mass Transfer]. *The CRC Handbook of Thermal Engineering*. [Kreith, F. (ed.)] [3-1–3-14] (CRC, Boca Raton, 2000).
18. Takahashi, K. *et al.* Bifunctional thermoelectric tube made of tilted multilayer material as an alternative to standard heat exchangers. *Sci. Rep.* **3**, 1501 (2013).

Acknowledgments

The authors thank Dr. D. Ueda for his enthusiastic encouragement of this work. This work was partially supported by the New Energy and Industrial Technology Development Organization (NEDO) of Japan.

Author contributions

A.S., H.T. and H.K. fabricated the BST/Ni multilayers. A.S. and K.T. measured the TE properties of the fabricated multilayers. A.S. analyzed the data based on a model developed by T.K. and drafted the manuscript, which was further revised by all authors. T.K. and Y.Y. directed the work. H.A. jointly discussed the experimental results.

Additional information

Supplementary information accompanies this paper at <http://www.nature.com/scientificreports>

Competing financial interests: The authors declare no competing financial interests.

How to cite this article: Sakai, A. *et al.* Breaking the trade-off between thermal and electrical conductivities in the thermoelectric material of an artificially tilted multilayer. *Sci. Rep.* **4**, 6089; DOI:10.1038/srep06089 (2014).



This work is licensed under a Creative Commons Attribution-NonCommercial-NoDerivs 4.0 International License. The images or other third party material in this article are included in the article's Creative Commons license, unless indicated otherwise in the credit line; if the material is not included under the Creative Commons license, users will need to obtain permission from the license holder in order to reproduce the material. To view a copy of this license, visit <http://creativecommons.org/licenses/by-nc-nd/4.0/>